LBL-33468
UC-408

Lawrence Berkeley Laboratory
UNIVERSITY OF CALIFORNIA

To be published as Chapter 9 in *Stereotactic Radiosurgery*,
E. Alexander, J.S. Loeffler, and L.D. Lunsford, Eds.,
McGraw-Hill, New York, NY, July 1993

Heavy-Charged-Particle Radiosurgery: Rationale and Method

K.A. Frankel, R.P. Levy, J.I. Fabrikant, and M.H. Phillips

July 1993

Donner Laboratory

Biology & Medicine Division

Prepared for the U.S. Department of Energy under Contract Number DE-AC03-76SF00098

DISCLAIMER

LBL-33468

Heavy-Charged-Particle Radiosurgery: Rationale and Method

Chapter 9
In E. Alexander, J.S. Loeffler, L.D. Lunsford (eds):
Stereotactic Radiosurgery
McGraw-Hill, New York, 1993

Kenneth A. Frankel, Ph.D.

Richard P. Levy, M.D., Ph.D.

Jacob I. Fabrikant, M.D., Ph.D.

Mark H. Phillips, Ph.D.

Life Sciences Division
Lawrence Berkeley Laboratory
University of California at Berkeley
Berkeley, CA 94720

July 1993

This research was supported by the Director, Office of Energy Research, Office of Health and Environmental Research, Medical Applications Division of the U.S. Department of Energy under Contract No. DE-AC03-76SF00098.

HEAVY-CHARGED-PARTICLE RADIOSURGERY: RATIONALE AND METHOD[1]

Kenneth A. Frankel, Ph.D.†, Richard P. Levy, M.D., Ph.D.‡, Jacob I. Fabrikant, M.D., Ph.D.°, and Mark H. Phillips, Ph.D.§

† Assistant Adjunct Professor of Radiology, University of California, San Francisco; Staff Scientist, Donner Pavilion and Donner Laboratory, Division of Life Sciences, Lawrence Berkeley Laboratory, University of California, Berkeley, California

‡ Assistant Adjunct Professor of Radiology, University of California, San Francisco; Medical Scientist and Staff Scientist, Donner Pavilion and Donner Laboratory, Division of Life Sciences, Lawrence Berkeley Laboratory, University of California, Berkeley, California

° Professor of Radiology, University of California, San Francisco and Berkeley; Medical Scientist and Senior Scientist, Donner Pavilion and Donner Laboratory, Division of Life Sciences, Lawrence Berkeley Laboratory, University of California, Berkeley, California

§ Associate Professor of Radiation Oncology, University of Washington Medical School, Seattle, Washington

Direct correspondence to:

Kenneth A. Frankel, Ph.D.
Donner Pavilion and Donner Laboratory
University of California at Berkeley
Berkeley, California 94720
Telephone: (510) 486-6149

Chapter Outline

[1]Research supported by the Director, Office of Energy, Health and Environmental Research of the United States Department of Energy under Contract DE-AC03-76SF00098.

HEAVY-CHARGED-PARTICLE RADIOSURGERY: RATIONALE AND METHOD[1]

INTRODUCTION

Heavy-charged-particle radiosurgery of the brain has been the subject of extensive clinical and basic research since 1954, when the first patients were irradiated at the University of California at Berkeley - Lawrence Berkeley Laboratory (UCB-LBL) 184-inch synchrocyclotron for pituitary-hormone-suppression treatment of metastatic breast cancer [1,2,3,4,5]. During the past four decades, the method of charged-particle radiosurgery has been progressively refined to reflect the concurrent theoretical and technical advances in physics, neuroradiology and computer science. This article describes: (1) the background and rationale for the use of charged-particle irradiation as a neurosurgical and/or radiotherapeutic procedure; (2) the current methods of treatment planning and dose delivery using Bragg-peak and plateau-beam irradiation; and (3) recent developments and future directions in the field of charged-particle radiosurgery.

PHYSICAL PROPERTIES OF CHARGED-PARTICLE BEAMS

Ionizing radiations used for stereotactic radiosurgery may be classified as high-energy photons (e.g., X-rays or gamma rays) or charged particles (e.g., protons or helium ions). The physical characteristics of both classes of radiation have been adapted for application to stereotactic radiosurgery, but in very different ways. As photons traverse and interact with tissue, their ionization events attenuate with depth in tissue (Fig. 9–1). Satisfactory dose distributions in deep-seated lesions are achieved, at the cost of a relatively high integral dose to the patient, by using beams from many different angles or intersecting dynamic arcs. Accelerated charged particles, including protons and helium ions, manifest very different

[1]Portions of this chapter are adapted with permission from: Levy RP, Fabrikant JI, Frankel KA, Phillips MH, Lyman JT: Charged-particle radiosurgery of the brain. Neurosurg Clin North Am 1:955–990, 1990, and from: Fabrikant JI, Levy RP, Steinberg GK, Phillips, MH, Frankel KA, Lyman JT, Marks MP, Silverberg GD: Charged-particle radiosurgery for intracranial vascular malformations. Neurosurg Clin North Am 3:99–139, 1992.

physical properties, first observed by Bragg in 1904 [6]. Beams of these charged particles have several physical properties that can be exploited to place a high dose of radiation preferentially within the boundaries of a deeply located intracranial target volume [3,7,8, 9,10,11,12]. These properties include: (1) a well-defined *range* that can be modulated so that the beam *stops* at the distal edge of the target and deep within the brain, resulting in little or no exit dose; (2) an initial region of low dose (the *plateau*) as the beam penetrates through tissue, followed by a region of high dose (the *Bragg ionization peak*) at the end of the range of the beam, which can be adjusted to conform to the location and dimensions of the target, so that the entrance dose can be kept to a minimum; and (3) very sharp lateral edges that can be shaped to conform to the projected cross-sectional contour of the target, so that negligible dose is absorbed by the adjacent normal tissues (Figs. 9–1, 9–2, 9–3).

Range

The distance or range that a charged particle travels in tissue before stopping is a function of the charge and kinetic energy of the particle, and of the physical characteristics of the absorbing tissue. Particle accelerators used for medical irradiation produce monoenergetic beams consisting of high-energy charged particles with ranges in tissue up to 30 cm or more. At the UCB-LBL Bevatron accelerator, the maximum usable range of the 165-MeV/u helium-ion beam is 15.5 cm in water [13]. This range is sufficient to treat most intracranial disorders, but beams of higher energies can be used if greater ranges are needed. The *residual range* (i.e., the distance in tissue the beam will traverse before stopping) can be adjusted precisely to stop the beam at the distal edge of the target volume by placing energy-absorbing material in the beam path.

Bragg–Peak and Plateau Ionization Regions

The Bragg ionization peak is a function of the rate of a charged particle's energy transfer to the tissue which it traverses. The radiation dose absorbed from a charged particle is relatively low in the initial plateau ionization region, increases gradually as the particle

slows, and then increases rapidly just before the particle stops, resulting in a large local energy deposition (the Bragg ionization peak) at the end of the particle's range (Figs. 9–1, 9–2). The *unmodulated* Bragg peak is just a few millimeters in width and, therefore, too narrow for the treatment of most intracranial lesions. However, the Bragg-peak width in the direction of the beam path can be spread-out (*modulated*) to any desired value, at the cost of some dose increase in the plateau region, by interposing variable-thickness absorbers in the beam path (e.g., by a rotating propeller or spiral ridge filter, or by adding together or dynamically "stacking" a sequential series of beams of slightly different ranges) (Fig. 9–1) [13,14]. Some dose deposition distal to the Bragg peak results from nuclear interactions between the incident particles and the atomic nuclei of the irradiated tissues; this dose is negligible for protons and helium ions, and it increases, due to nuclear fragmentation, for heavier charged particles (e.g., carbon or neon ions) [15]. At the Bevatron, distal dose fall-off to 10% of the central axis dose occurs within 2 to 3 mm for the 165 MeV/u helium-ion beam [13].

Transverse Beam Profile

A sharp transverse beam profile is desirable to minimize the dose to the normal tissues immediately adjacent to the target volume. The measured lateral *penumbra* (distance between the 90% and 10% dose profiles) for the 165 MeV/u helium-ion beam at the Bevatron is 3.5 mm at 9-cm depth in water, and it increases to 4.5 mm at 12 cm-depth (Fig. 9–2) [13]. Charged-particle beams are readily collimated by beam-shaping apertures. When small lesions are treated, the beams generally are collimated with either circular or elliptical brass apertures. With larger and/or irregularly shaped lesions, individually designed apertures are fabricated from cerrobend (a low-melting-temperature dense alloy) to collimate the beam shape in accordance with the cross-sectional size and shape of the target volume (Fig. 9–3) [3,16].

BRAGG–PEAK METHOD: ARTERIOVENOUS MALFORMATIONS

The application of heavy-charged-particle Bragg peak radiosurgery to the treatment of intracranial vascular and other disorders presents a number of problems not encountered in conventional radiotherapy treatment planning [17,18]. To utilize fully the unique physical characteristics of the charged-particle beams for safe and effective treatment, the target volume must be defined and located precisely within a reproducible three-dimensional frame of reference, the physical properties of the materials to be traversed by the beam must be determined accurately, and the patient must be positioned exactly with respect to the beam [16,19]. Treatment planning consists of a series of stages involving sequential stereotactic neuroradiologic imaging studies, computer-assisted correlations among the different types of radiologic imaging information and calculations of the dose distributions. In this section, we consider Bragg-peak radiosurgery for arteriovenous malformations (AVMs), a condition for which cerebral angiography plays a major role in target definition and localization [3,7,16,20,21,22,23,24]. Many aspects of the methods described in this section, however, are also applicable to the treatment of other intracranial disorders for which angiography is of little or no value; the radiosurgical approach to these conditions will be described briefly in subsequent sections.

Stereotactic Immobilization System

We have developed a transportable stereotactic frame-mask system that permits accurate and reproducible positioning of the patient's head for neuroradiologic procedures, including target definition and localization, complex treatment planning and single-fraction or multifraction radiosurgical treatment (Fig. 9–4) [19,25]. This frame-mask system consists of an individualized thermoplastic immobilizing head mask and stereotactic frame. The stereotactic frame has fiducial markers for three-dimensional localization and image correlation, and it can be attached to the requisite neuroradiologic imaging couches and to the stereotactic positioning couch – the Irradiation Stereotactic Apparatus for Humans

(ISAH) (Fig. 9–5) [25,26]. ISAH has three degrees of freedom for translation, two degrees of freedom for rotation (the third degree of rotational freedom is effected by rotation of the beam-shaping aperture) and a mechanical precision of 0.1 mm and 0.1°. Based upon the limits of resolution of neuroradiologic imaging data and image correlation and the intrinsic uncertainties in patient positioning, the overall localization and alignment system is reproducible in repeated diagnostic and therapeutic sessions to approximately 1.5 mm and 1.5° in each translational and rotational degree of freedom, respectively [16,19,25]. This system has proven to be safe and reliable in more than 1300 patients [3,25].

Neuroradiologic Evaluation and Image Correlation

Stereotactic neuroradiologic evaluation for AVMs includes cerebral angiography, computed X-ray tomography (CT) scans and magnetic resonance imaging (MRI) scans. The composite information from these studies is used to determine the radiosurgical target and treatment volume. Stereotactic angiography is the most precise imaging method for determining the size, shape and location of an AVM. However, CT data are required for charged-particle-beam range calculations, and MRI and CT imaging are best for demonstrating relationships of the lesion to adjacent anatomic structures.

The stereotactic frame and head-immobilization system are used to correlate the multivessel angiographic and CT images [16,25]. The contours of the AVM target, derived from selected orthogonal angiographic films and transferred to the noncontrast CT images, form the basis for the stereotactic treatment-planning procedure. Via geometric optics, a computerized digitization program (developed at LBL) uses the positions of the fiducial markers of the stereotactic frame as they appear on the radiographs, in conjunction with their known positions on the frame, to calculate radiographic magnification factors, the size of the AVM and the coordinates of the target volume within the frame (Fig. 9–6) [16]. The digitized angiographic data are also used to calculate the initial translational coordinates of the patient-positioning couch and to provide the basis for appropriately magnified computer-generated overlays (alignment aids) of the stereotactic-frame fiducial markers,

angiographically derived target contours and midplane bony landmarks of the skull for lateral and anteroposterior localization radiographs (see Section on Target Localization and Treatment Procedure) [16].

The digitization program also models the angiographically derived AVM target volume as a series of ellipses on corresponding axial CT slices (see below). The CT data and derived target contours for each axial CT slice are reformatted to generate relevant views in coronal and sagittal planes. The reformatted target contours, which are corrected for parallax and magnification, then have approximately the same shape and location as the AVM target delineated on the orthogonal angiographic films [16].

Noncontrast stereotactic CT data are loaded into a VAX computer (Digital Equipment Corp., Maynard, MA), and the coordinates (row, column and CT slice number) of the ends of two of the wire fiducial markers on the stereotactic frame are obtained. This information, along with the CT-slice thickness (3 mm) and pixel size (typically, 0.8 to 1 mm), is used to map the angiographically determined digitized target contours onto the CT-image data set [16]. At each level of the angiographic image (along the cranial-caudal axis) that corresponds to a CT slice, the dimensions of the anteroposterior and lateral projections of the AVM are used as the major and minor axes of an ellipse. Thus, the AVM target volume in the CT-image set consists of a series of ellipses, stacked one on top of the other, each of thickness equal to the CT-slice separation. Occasionally, these elliptical contours deviate significantly from the true shape of the lesion, as indicated by CT or MRI studies, such as when the AVM closely follows the edge of some clearly defined anatomic structure. In these cases, the CT-target contours are revised to conform to the observed target geometry (see Section on New Developments and Future Directions).

For a homogeneous tissue, positioning the Bragg peak at a specified depth is quite straightforward. However, if the tissues are heterogeneous, as are the tissues of the skull and brain, the procedure is more complex [17,18]. Generally, denser bone tissue slows the incident stream of charged particles more per unit length of tissue than does less dense

parenchymal tissue. Thus, a beam traversing denser tissue will have its Bragg-peak region displaced proximally to a greater extent than a beam traversing less dense tissue. Knowledge of the composition of each volume element of tissue along the beam path is necessary for precise determination of dose distribution and for calculating the depth of penetration of the beam. The noncontrast CT data provide information regarding the physical characteristics of the tissues on a pixel-by-pixel basis by providing electron-density data (X-ray absorption coefficients), which are converted to charged-particle energy loss by established calibration functions [17]. Further adjustment of the beam range with individually shaped tissue-equivalent compensators positioned in the beam path is used to accommodate irregularly shaped lesions and skull curvature (Fig. 9–5) [22]. For most lesions, lucite compensators, shaped as triangular wedges and/or rectangular parallelepipeds, suffice to match the distal edge of the spread-out Bragg peak (across the transverse profile of the beam) to the distal surface of the target volume [3,16,18].

Computer-Assisted Treatment Planning

The size, shape and location of the lesion, the total dose to the target volume and the dose to adjacent normal brain structures are interrelated factors that affect the choice of beam ports, entry angles and dose-configuration patterns. Several prospective treatment plans (isodose-contour displays) are calculated individually for each patient. The final treatment plan is selected after iterative refinement of a number of preliminary treatment plans.

Each charged-particle beam can be directed to place individually shaped three-dimensional high-dose regions precisely within the brain by adjusting the range, by spreading the Bragg peak, by introducing tissue-equivalent compensators and by using an appropriately shaped aperture (Fig. 9–5). Several entry angles and beam ports (usually, four) are directed stereotactically so that the high-dose regions of the individual beams intersect within the target volume, ensuring a relatively homogeneous dose distribution with the 90% isodose surface contoured to the edge of the target volume to the extent possible, with a much lower

dose to immediately adjacent and intervening normal brain tissues [3,7,20,21,23]. Figures 9–7 and 9–8 are representative examples of the isodose-contour displays of treatment plans for small and large AVMs, respectively.

A computer-assisted treatment-planning program (developed at LBL) is used to calculate dose distributions and to generate isodose curves [17]. Treatment planning is generally performed on the central CT-target slice (axial, coronal and sagittal views), but it can be performed on other CT slices if desired. For near-ellipsoidal target volumes smaller than 50 cm^3, treatment planning limited to the central CT slice is usually sufficient. The beam angles and selected doses[2] for all beam ports are entered into the treatment-planning program, which automatically calculates the required parameters for transverse beam width, beam range and spread of the Bragg peak. The program-derived parameters may subsequently be modified to individualize the treatment plan. The composite dose distributions and corresponding isodose-display curves are generated for each CT slice and plane of interest.

Charged–Particle Dosimetry

At the Bevatron ISAH facility, a series of beam-monitoring and dosimetry tests are performed before treatment to verify the reliability of the system. First, the charged-particle beam is delivered to the treatment room and tuned to an optimal focus and uniformity. Daily dosimetry measurements are performed and compared with a reference value. Following this procedure, the beam range, which can vary about 1.0 to 1.5 mm on a day-to-day basis, is measured. A test treatment for one of the day's scheduled beam ports is performed, using a reference ionization chamber (Far West Technology, Model IC-17A), which is placed at isocenter and given a prescribed dose. The dose measured is usually within 2% of the value expected based on previously established calibration factors (see below). Discrepan-

[2]The Gray-equivalent (GyE) dose is the physical dose (in Gy) multiplied by a factor to account for the increased relative biologic effectiveness (RBE) of the Bragg ionization peak of the charged-particle beam. The RBE for cell killing in the helium-ion (165 MeV/u) spread-out Bragg peak is approximately 1.3, i.e., it is approximately 30% more effective than 225-kVp X-rays in killing proliferating cells, based on *in vitro* and *in vivo* studies [27].

cies greater than 2% are usually due to daily fluctuations in the magnet settings for the beam focus (which can result in the beam having a slightly different shape or direction than expected), in which case the beam ports must be calibrated individually.

A wire chamber, two plane-parallel ionization chambers and a secondary emission monitor are used to localize the central axis of the beam and to measure the intensity, profile and size of the beam [13,28,29,30,31,32]. The residual range and spreading-out of the Bragg peak are adjusted with a variable-thickness water absorber [13,33]. In the standard beamline configuration, the Bragg-peak width can be spread-out from 5 to 35 mm in 5-mm increments; other peak-spreading configurations are available as required.

Each beam port used for treatment is characterized by the parameters of residual range, spread-out Bragg-peak width and selected dose. Each set of beam-port parameters requires that a specific array of settings be loaded into dose-counting scalers that automatically turn off the beam when their values have been reached [13]. The entire system has been calibrated for the values of residual range and spread-out Bragg-peak width currently in use. Calibration factors (derived from dose-measuring devices) have been fit to polynomial functions, which are used to calculate the required scaler settings for each beam port prior to treatment.

The beam intensity and focus are monitored continuously during patient treatment. The counts for the two ionization chambers and secondary emission monitor generally agree within 2% of that expected by the scalers. Discrepancies greater than 2% are investigated and corrected before treatment proceeds [13].

Target Localization and Treatment Procedure

The radiosurgical procedure requires that the target volume be localized precisely at the intersection of the charged-particle beam and the isocenter of ISAH [26]. A simulation of the treatment procedure is carried out before treatment to verify the accuracy of stereotactic localization and to anticipate any problems with patient positioning and compliance. At the simulation, the patient is positioned (at the coordinates specified by the digitization

program) in the stereotactic frame-mask system, which is attached to ISAH. Alignment of the patient's head (and the AVM target) is verified by comparing the orthogonal lateral and anteroposterior localization radiographs, taken with the patient immobilized on ISAH, to the computer-generated digitized overlays of the frame, skull and angiographically determined target volume (Fig. 9–6) [16]. At this time, the patient is moved sequentially to all contemplated treatment positions to preclude any unforeseen positioning problems that might arise during treatment.

At treatment, the patient is repositioned on ISAH in the stereotactic frame-mask system and orthogonal localization radiographs are repeated. The localization radiograph perpendicular to the charged-particle beam path is also exposed to a low-dose beam shaped by the aperture to be used for that beam port. The resulting *port film* and localization radiographs are compared to the digitized overlays, and necessary adjustments of patient-positioning and aperture rotation are made. The process is repeated, as required, until satisfactory alignment is achieved. Once the target center is positioned at the isocenter of ISAH, the treatment beams are delivered through a number of ports by rotating the patient's head and/or treatment couch sequentially to predetermined fixed positions [3,7,20,21,23]. The target-localization procedure is repeated prior to treatment for each required set of positioning coordinates (e.g., for anterior, posterior and lateral beam ports). The entire radiosurgical procedure typically requires about 30 to 60 minutes; each beam port requires 10 to 15 minutes for patient positioning, aperture adjustment and compensator placement and 1 to 3 minutes for beam exposure. All patients are treated on an outpatient basis.

BRAGG–PEAK METHOD: OTHER DISORDERS

Angiographically Occult Vascular Malformations

We have developed methods for correlating stereotactic MRI and CT images to determine the location, size and shape of the target volume for treatment planning of intracranial conditions in which angiography does not contribute substantially to target definition and

localization (e.g., angiographically occult vascular malformations (AOVMs) and/or neoplastic disorders) [19,34,35,36]. These methods, described here for the radiosurgical treatment of AOVMs, are also directly applicable to the treatment of intracranial neoplasms. In the patient whose treatment planning is illustrated in Fig. 9–9, the AOVM in the brain stem is clearly demonstrated on MRI. Radiosurgical target contours are delineated on stereotactic MRI and CT images. The MRI-derived target contours are transferred to CT for comparison with CT-derived contours, and a final set of target contours is then defined on the CT images. For each CT slice, the inner and outer tables of the skull are digitized, along with selected other bony landmarks, such as the pituitary sella, frontal plates and anterior and posterior protuberances. A computer program (developed at LBL) then generates CT-derived treatment-localization overlays, based on the final target contours and the digitized bony landmarks. The stereotactic CT data are also used to determine the initial coordinates required to position the patient on ISAH.

Final positioning of the patient for treatment is based on comparison of localization radiographs and port films with the treatment overlays. Treatment plans and isodose contours are developed on the relevant CT slices in a similar manner to that used for AVMs (see Section on Computer-Assisted Treatment Planning, above). The resulting isodose contours may then be transferred back to MRI to examine the dose to the AOVM and other brain structures of interest.

Pituitary Adenomas

The radiosurgical treatment of pituitary adenomas represents a special situation for which the localization procedure is greatly simplified, because the sella turcica is midline and it can usually be readily identified and localized on plain radiographs. Since pituitary adenomas are approximately midline, parallax corrections for localization on stereotactic simulation radiographs are insignificant. Stereotactic sagittal and coronal MRI views through the sella, therefore, can be magnified to correspond precisely to the respective orthogonal lateral and anteroposterior localization radiographs and port films. Thus, the

contours of the tumor volume and adjacent structures of interest can be transferred (traced) directly onto the localization radiographs performed at the simulation. Concurrently, these contours are transferred to corresponding CT slices, where treatment planning proceeds in a similar manner to that described earlier for AVMs (see Section on Computer-Assisted Treatment Planning, above). Final alignment of the patient is verified by comparing the localization radiographs and port films exposed immediately prior to treatment to the localization radiographs (now modified to include the target contours) taken during the simulation procedure.

In Fig. 9–10, an acromegalic tumor with extension to the left cavernous sinus and its relationships to adjacent neural structures are defined on stereotactic MRI scans, and the radiosurgical target is delineated. The treatment plan is designed to minimize the dose to the structures of the cavernous sinus while placing a higher dose in the portion of the tumor mass lying within the sella (Fig. 9–11). Generally, eight noncoplanar beam ports are used to effect a favorable dose distribution.

PLATEAU-BEAM STEREOTACTIC IRRADIATION

When a charged-particle beam of sufficiently high energy, and hence greater depth of penetration, is available, radiosurgery can be performed with the plateau-ionization portion of the beam. In this treatment configuration, the beam passes completely through the head, depositing plateau-region radiation in the brain (Fig. 9–12); the Bragg-peak dose is absorbed in the wall of the the treatment room opposite the beam line. This method was developed by Lawrence and his colleagues [4,5,37,38,39] at UCB-LBL in 1954 for irradiation of the pituitary gland with plateau beams of protons and helium ions, and it is currently applied to radiosurgery of small intracranial target volumes at several proton-irradiation centers in Russia (see also Chapter 12) [40,41,42,43,44,45].

With the plateau-beam-irradiation technique, consideration of the tissue inhomogeneity normally encountered in the head is not important, but accurate stereotactic localization of

the intracranial target volume and precise isocentric technique are essential. The plateau-beam radiosurgical system developed at UCB-LBL uses a stereotactic positioning table and head holder in combination with individually fabricated plastic head masks for immobilization (Fig. 9–12). Following delineation of the target volume, the charged-particle beam is centered on the sella turcica by means of orthogonal localization radiographs and port films, and the beam contour is shaped by a brass aperture. During irradiation, the head is turned in pendulum motion around a horizontal axis while the patient is positioned sequentially at 12 discrete angles around a vertical axis (Fig. 9–12). The irradiation arcs are directed such that the dose fall-off is very rapid in the anteroposterior direction and toward the optic chiasm; the dose fall-off decreases more slowly laterally toward the temporal lobes (Fig. 9–13). With this method, the optic chiasm, hypothalamus and outer portions of the sphenoid sinus receive less than 10% of the central-axis pituitary dose [39]. For small lesions, the dose distributions from plateau-beam irradiation are comparable to those produced with stereotactic radiosurgical systems using X-rays or gamma rays.

Plateau-beam radiosurgery can also be used for the treatment of disorders other than pituitary adenomas. For these applications, however, it is necessary to incorporate the more-general methods of stereotactic target localization described in previous sections of this chapter.

NEW DEVELOPMENTS AND FUTURE DIRECTIONS

Large or Irregularly Shaped Lesions

In our experience, most AVMs can be modeled, with only minor modifications, as a series of ellipses on adjacent CT slices (see Section on Neuroradiologic Evaluation and Image Correlation, above). Treatment of these lesions generally requires aperture designs based on orthogonal angiographic projections and the use of simple lucite compensators. With some large or irregularly shaped AVMs, however, the projection of the angiographically defined AVM contours onto corresponding CT slices yields target contours that are inconsistent

with the AVM contours suggested by diagnostic CT and MRI scans [11]. In these cases, significant modifications of the angiographically derived target contours may be required to preclude inadvertently targetting normal brain structures for irradiation (Fig. 9–14). Beam-shaping apertures and localization overlays must be designed individually for each beam port, including those at oblique angles. Additionally, tissue-compensators must be designed on a CT-slice-by-slice basis.

The first stage in this complex procedure is the delineation of preliminary targets for all relevant angiographic studies in orthogonal lateral and anteroposterior views. For large and complex lesions, the target contours derived from stereotactic angiography must be digitized individually for each contrast-injected vessel. The next stage requires that preliminary target contours also be delineated on diagnostic stereotactic CT and MRI scans on a slice-by-slice basis. The preliminary target contours for the imaging studies are then transferred to the corresponding noncontrast-CT data set. The target contours derived from CT and MRI studies should lie completely within (and abut) the orthogonally oriented rectangles that circumscribe the angiographically defined elliptical targets (see Section on Neuroradiologic Evaluation and Image Correlation, above) [11,16,19,22]. If these target-correlation criteria are not met, then it is necessary to revise the preliminary target contours. Final decisions on the target contours must be based on clinical judgment using composite information from all available imaging studies, since no single study provides the complete three-dimensional information needed to determine the appropriate target volume. In practice, an iterative approach of target refinement and image correlation is used until a final set of target contours is obtained that is consistent in all imaging modalities. The final set of target contours is now used, in conjunction with angiographic and CT data, respectively, to generate two sets of treatment-localization overlays (see Sections on Neuroradiologic Evaluation and Image Correlation and Angiographically Occult Vascular Malformations, above). The CT-derived lateral and anteroposterior overlays are checked for consistency with the corresponding angiographically derived overlays. (If oblique beam ports are used,

the overlays are generated based on CT-scan data alone.) The size and shape of the beam collimators are based on the composite angiographic and CT contours.

Tissue-equivalent compensators, which can be constructed from lucite or wax, are designed on a CT-slice-by-slice basis for each beam port as an integral part of the computer-assisted treatment-planning procedure [17]. For fabrication of wax compensators, the data file that contains the compensator-design information is electronically transferred to a computer-controlled milling machine. In the case of lucite compensators, the computer program generates a print-out of the required shape of each compensator on a CT-slice-by-slice basis; these print-outs are then used to guide machining of the compensators. A representative isodose-contour display demonstrating the composite (multi-port) compensator-integrated treatment plan for a large and irregularly shaped AVM is shown in Fig. 9–14; computer-designed wax compensators were used to minimize dose to the right thalamus and other adjacent structures. Four coplanar beam ports were used – one anterior, one posterior and two from the patient's right side at $\pm 30°$.

Beam Scanning

In the standard radiosurgery-beamline configuration at the Bevatron, each beam port is characterized by a fixed value of the spread-out Bragg peak that corresponds to the greatest extent of the target volume in the direction of the beam path. Currently, lesions with substantial variation of width in the direction of the beam path may be treated using multiple isocenters. If several isocenters are required, however, it may be difficult to achieve a uniform dose distribution through the target volume while minimizing the dose to adjacent normal tissues. An alternative approach, currently being tested at LBL, is to utilize a *beam-scanning* system, whereby the charged-particle beam is swept step-wise across the target volume by a computer-controlled magnetic field. In this approach, the target volume is subdivided into multiple sections. In turn, each section of the target volume is irradiated with a charged-particle beam characterized by a specific value of the spread-out Bragg-peak width optimized to correspond to that section. The beam-scanning system will be used in

conjunction with a computer-controlled multi-leaf collimator which dynamically adjusts the beam collimation to the shape of the projected target area. This new system should provide improved dose distributions for large, irregularly shaped lesions, and it should prove to be especially useful for reducing the dose to critical brain structures which may partially be enclosed by concave target volumes (Fig. 9–15).

SUMMARY

Heavy-charged-particle beams manifest unique physical properties which are advantageous for application to the radiosurgical treatment of intracranial disorders. These properties include a finite range, a Bragg ionization peak and a sharp lateral penumbra. Charged-particle radiosurgery can be applied effectively using either the Bragg-peak method, in which the charged particles *stop* within the target volume, or the plateau-beam method, in which the charged particles pass completely through the patient's head.

At the University of California at Berkeley - Lawrence Berkeley Laboratory, neuroradiologic evaluation for charged-particle radiosurgery is conducted with the patient immobilized in a removable head mask and stereotactic frame. A series of imaging studies, which may include cerebral angiography and CT and MRI scans, are used to develop an integrated set of target contours for CT-based treatment planning. A computer-assisted treatment-planning procedure is used to select the appropriate beam-port parameters, including the beam-entry angles and the corresponding beam ranges, spread-out Bragg-peak widths and aperture sizes. From these parameters, the treatment-planning program calculates the dose distribution on a CT-slice-by-slice basis, generates corresponding isodose-contour displays and designs tissue-equivalent compensators required to conform the distal edge of the Bragg peak to the target contour. The treatment-planning program also constructs treatment-localization overlays for verification of patient positioning at treatment.

Recent developments, which are expected to provide improved dose distributions, especially for large and/or irregularly shaped lesions, include the incorporation of new methods

for target definition, compensator design and beam delivery. These new methods include: (1) iterative target definition based on the composite imaging information derived from stereotactic angiography and CT and MRI scans; (2) CT-slice-by-slice compensator design; and (3) the use of a beam-scanning system to adjust the spread-out Bragg-peak width dynamically as the charged-particle beam sweeps across the target volume.

ACKNOWLEDGMENTS

The authors wish to acknowledge Professors J. H. Lawrence (deceased), C. A. Tobias and J. T. Lyman for their pioneering contributions to the field of charged-particle radiosurgery. Research supported by Director, Office of Health and Environmental Research, U. S. Department of Energy under Contract No. DE-ACO3-76SF00098.

References

[1] Brobeck WM, Lawrence EO, MacKenzie KR, McMillan EM, Serber R, Sewall DC, Simpson KM, Thornton RL: Initial performance of the 184-inch cyclotron of the University of California. Phys Rev 71:449–450, 1947

[2] Lawrence JH: Proton irradiation of the pituitary. Cancer 10:795–798, 1957

[3] Levy RP, Fabrikant JI, Frankel KA, Phillips MH, Lyman JT: Charged-particle radiosurgery of the brain. Neurosurg Clin North Am 1:955–990, 1990

[4] Tobias CA, Lawrence JH, Born JL, McCombs RK, Roberts JE, Anger HO, Low-Beer BVA, Huggins CB: Pituitary irradiation with high-energy proton beams: A preliminary report. Cancer Res 18:121–134, 1958

[5] Tobias CA, Roberts JE, Lawrence JH, Low-Beer BVA, Anger HO, Born JL, McCombs R, Huggins CB: Irradiation hypophysectomy and related studies using 340-MeV protons and 190-MeV deuterons. *In* Proceedings of the International Conference on the Peaceful Uses of Atomic Energy, Geneva, 1955, pp 95–106

[6] Bragg WH, Kleeman RD: On the ionization curves of radium. Philosoph Mag 8:726–738, 1904

[7] Fabrikant JI, Levy RP, Steinberg GK, Phillips MH, Frankel KA, Lyman JT, Marks MP, Silverberg GD: Charged-particle radiosurgery for intravascular malformations. Neurosurg Clin North Am 3:99–139, 1992

[8] Larsson B, Leksell L, Rexed B, Sourander P, Mair W, Andersson B: The high-energy proton beam as a neurosurgical tool. Nature 182:1222–1223, 1958

[9] Leksell L, Larsson B, Andersson B, Rexed R, Sourander P, Mair W: Lesions in the depth of the brain produced by a beam of high energy protons. Acta Radiol 54:251–264, 1960

[10] Lyman JT, Frankel KA, Phillips MH, Levy RP, Fabrikant JI: Radiation physics for particle beam radiosurgery. Neurosurg Clin North Am 3:1–7, 1992

[11] Phillips MH, Frankel KA, Lyman JT, Fabrikant JI, Levy RP: Comparison of different radiation types and irradiation geometries in stereotactic radiosurgery. Int J Radiat Oncol Biol Phys 18:211–220, 1990

[12] Wilson RR: Radiological use of fast protons. Radiology 47:487–491, 1946

[13] Ludewigt BA, Chu WT, Phillips MH, Renner TR: Accelerated helium-ion beams for radiotherapy and stereotactic radiosurgery. Med Phys 18:36–42, 1991

[14] Lyman JT, Kanstein L, Yeater F, Fabrikant JI, Frankel KA: A helium-ion beam for stereotactic radiosurgery of central nervous system disorders. Med Phys 13:695–699, 1986

[15] Lyman JT, Fabrikant JI, Frankel KA: Charged-particle stereotactic radiosurgery. Nucl Instrum Methods Phys Res B10/11:1107–1110, 1985

[16] Phillips MH, Frankel KA, Lyman JT, Fabrikant JI, Levy RP: Heavy-charged particle stereotactic radiosurgery: Cerebral angiography and CT in the treatment of intracranial vascular malformations. Int J Radiat Oncol Biol Phys 17:419–426, 1989

[17] Chen GTY, Singh RP, Castro JR, Lyman JT, Quivey JM: Treatment planning for heavy ion radiotherapy. Int J Radiat Oncol Biol Phys 5:1809–1819, 1979

[18] Verhey L, Goitein M: Problems of inhomogeneities in particle beam therapy. *In* Skarsgard LD (ed): Pion and Heavy-Ion Radiotherapy. Pre-Clinical and Clinical Studies. New York, Elsevier Biomedical, 1983, pp 159–168

[19] Phillips MH, Kessler M, Chuang FYS, Frankel KA, Lyman JT, Fabrikant JI, Levy RP: Image correlation of MRI and CT in treatment planning for radiosurgery of intracranial vascular malformations. Int J Radiat Oncol Biol Phys 20:881–889, 1991

[20] Fabrikant JI, Lyman JT, Frankel KA: Heavy charged-particle Bragg peak radiosurgery for intracranial vascular disorders. Radiat Res [Suppl] 104:S244–S258, 1985

[21] Fabrikant JI, Lyman JT, Hosobuchi Y: Stereotactic heavy-ion Bragg peak radiosurgery: Method for treatment of deep arteriovenous malformations. Br J Radiol 57:479–490, 1984

[22] Frankel KA, Phillips MH, Lyman JT, Chuang FYS, Fabrikant JI, Levy RP, Rosander K: Treatment planning for stereotactic heavy-charged-particle radiosurgery of the brain. *In* Steiner L (ed): Radiosurgery: Baselines and Trends, New York, Raven Press, 1992, pp 75–83

[23] Levy RP, Fabrikant JI, Frankel KA, Phillips MP, Lyman JT: Stereotactic heavy-charged-particle Bragg peak radiosurgery for the treatment of intracranial arteriovenous malformations in childhood and adolescence. Neurosurgery 24:841–852, 1989

[24] Steinberg GK, Fabrikant JI, Marks MP, Levy RP, Frankel KA, Phillips MH, Shuer LM, Silverberg GD: Stereotactic heavy-charged-particle Bragg-peak radiation for intracranial vascular malformations. N Engl J Med 323:96–101, 1990

[25] Lyman JT, Phillips MH, Frankel KA, Fabrikant JI: Stereotactic frame for neuroradiology and charged particle Bragg peak radiosurgery of intracranial disorders. Int J Radiat Oncol Biol Phys 16:1615–1621, 1989

[26] Lyman JT, Chong CY: ISAH: A versatile treatment positioner for external radiation therapy. Cancer 34:12–16, 1974

[27] Blakely EA, Ngo FQH, Curtis SB, Tobias CA: Heavy-ion radiobiology: Cellular studies. *In* Lett JT (ed): Advances in Radiation Biology (vol. 11), New York, Academic Press, 1984, pp 295–389

[28] Boag JW: Ionization chambers. *In* Attix FU, Roesch WC, Tochlin E (eds): Radiation Dosimetry (vol. 2), New York, Academic Press, 1966, pp 1–72

[29] Lyman JT, Howard J: Dosimetry and instrumentation for helium and heavy ions. Int J Radiat Oncol Biol Phys 3:81–85, 1977

[30] Renner TR, Chu WT: Wobbler facility for biomedical experiments. Med Phys 14:825–834, 1987

[31] Renner TR, Chu WT, Ludewigt BL, Nyman MA, Stradtner R: Multisegmented ionization chamber dosimetry system for light ion beams. Nucl Instrum Methods A281:640–648, 1989

[32] Tautfest GW, Fechter HR: A nonsaturable high-energy beam monitor. Rev Sci Instrum 26:229–231, 1955

[33] Tobias CA, Lyman JT, Chatterjee A, Howard J, Maccabee HD, Raju MR, Smith AR, Sperinde JM, Welsch GP: Radiological physics characteristics of the extracted heavy ion beams of the Bevatron. Science 174:1131–1134, 1971

[34] Kessler ML: Integration of multimodality imaging data for radiotherapy treatment planning. Ph.D. Thesis. Berkeley, University of California, 1989

[35] Kessler ML, Pitluck S, Petti P, Castro JR: Integration of multimodality imaging data for radiotherapy treatment planning. Int J Radiat Oncol Biol Phys 21:1653–67, 1991

[36] Levy RP, Fabrikant JI, Phillips MH, Frankel KA, Steinberg GK, Marks MP, DeLaPaz RL, Chuang FYS, Lyman JT: Clinical results of stereotactic heavy-charged-particle radiosurgery for intracranial angiographically occult vascular malformations. *In* Steiner L (ed): Radiosurgery: Baselines and Trends, New York, Raven Press, 1992, pp 221–228

[37] Lawrence JH, Born JL, Tobias CA, Carlson R, Sangalli F, Welch G: Clinical and metabolic studies in patients after alpha particle subtotal or total hypophysectomy. *In* Medicine in Japan in 1959. Proceedings of the 15th General Assembly of the Japan Medical Congress, Tokyo, 1959, pp 859–862

[38] Lawrence JH, Tobias CA, Linfoot JA, Born JL, Gottschalk A, Kling RP: Heavy particles, the Bragg curve and suppression of pituitary function in diabetic retinopathy. Diabetes 12:490–501, 1963

[39] Tobias CA: Pituitary radiation: Radiation physics and biology. *In* Linfoot JA (ed): Recent Advances in the Diagnosis and Treatment of Pituitary Tumors, New York, Raven Press, 1979, pp 221–243

[40] Konnov B, Melnikov L, Zargarova O, Lebedeva L, Yalynych N, Karlin D: Narrow proton beam therapy for intracranial lesions. *In* International Workshop on Proton and Narrow Photon Beam Therapy, Oulu, Finland, 1989, pp 48–55

[41] Minakova YeI: Review of twenty years proton therapy clinical experience in Moscow. *In* Proceedings of the Second International Charged Particle Workshop, Loma Linda, CA, 1987, pp 1–23

[42] Minakova YeI: Twenty years clinical experience of narrow proton beam therapy in Moscow. *In* Proceedings of the International Heavy Particle Therapy Workshop, Paul Scherrer Institute, Villigen, Switzerland, 1990, pp 158–162

[43] Minakova YeI, Kirpatovskaya LYe, Lyass FM, Snigiryova RYa, Krymsky VA: Proton therapy of pituitary adenomas. Med Radiol (Mosk) 28 (10):7–13, 1983 (in Russian)

[44] Minakova YeI, Krymsky VA, Luchin YeI, Serbinenko FA, Lyass FM, Gabibov GA: Proton beam therapy in neurosurgical clinical practice. Med Radiol (Mosk) 32 (8):36–42, 1987 (in Russian)

[45] Minakova YeI, Vasil'eva NN, Svyatukhina OV: Irradiation of the hypophysis with single large dose of high energy protons for advanced breast carcinoma. Med Radiol (Mosk) 22 (1):33–39, 1977 (in Russian)

FIGURE LEGENDS

Fig. 9–1. Relative dose in water as a function of depth is shown for 8-MeV photons (dotted line), an *unmodulated* helium-ion (165 MeV/u) beam (solid line) and a helium-ion beam with a spread-out Bragg peak (SOBP) *modulated* to 2-cm width (dashed line) by interposing variable-thickness absorbers in the beam path. The unmodulated Bragg peak produces a narrow beam with high energy deposition at the end of the range, suitable for producing small intracranial lesions. For most radiosurgical applications, it is necessary to spread-out the width of the Bragg peak to ensure optimum dose distribution throughout the lesion. (*From* Levy RP, Fabrikant JI, Frankel KA, Phillips MH, Lyman JT: Charged-particle radiosurgery of the brain. Neurosurg Clin North Am 1:958, 1990.) [XBL 901-331A]

Fig. 9–2. The Bragg ionization curve and its transverse profile for the 165-MeV/u helium-ion beam at the University of California at Berkeley - Lawrence Berkeley Laboratory Bevatron. **Left**, the Bragg-peak-to-plateau dose ratio is approximately three, and the relative biologic effectiveness in the peak is estimated to be about 1.3; thus, the biologic effect in the peak is about four times that in the plateau region. Dose fall-off from 90% to 10% occurs within 2 to 3 mm distal to the Bragg peak. **Right**, the transverse profile of the Bragg peak demonstrates sharp edges; the lateral dose fall-off from 90% to 10% occurs within 2.5 mm. This profile was measured 1 cm proximal to the distal edge of a beam with a 7-cm residual range and with the Bragg peak spread 2 cm. Distal and lateral dose fall-off are negligibly affected by spreading the Bragg peak. (*From* Fabrikant JI, Levy RP, Steinberg GK, Phillips MH, Frankel KA, Lyman JT, Marks MP, Silverberg GD: Charged-particle radiosurgery for intracranial vascular malformations. Neurosurg Clin North Am 3:102, 1992.) [XBL 9012-3874]

Fig. 9–3. Charged-particle beams can be readily contoured by metal apertures shaped to conform to the cross-sectional size and shape of the target volume in any projection. **Upper**, a lateral projection view of a stereotactic cerebral angiogram (left internal carotid

artery injection) demonstrates a large arteriovenous malformation occupying the genu and body of the corpus callosum. The composite radiosurgical target, selected after evaluation of the multivessel cerebral angiogram study, has been outlined (see arrowheads). **Lower**, an individually tailored brass and cerrobend aperture has been fabricated from computer-defined contours derived from the cerebral angiogram to conform to the radiosurgical target in the corpus callosum. The aperture is inserted into the beam line for appropriate shaping of the lateral beams during radiosurgery (cf Fig. 9–5). (*From* Levy RP, Fabrikant JI, Frankel KA, Phillips MH, Lyman JT: Charged-particle radiosurgery of the brain. Neurosurg Clin North Am 1:962, 1990.) [XBB 901-795A]

Fig. 9–4. Stereotactic frame and patient mask system (cf Fig. 9–5). The head-immobilization mask is formed of thermoplastic material, and it is molded individually for each patient's head. Letters denote components of the stereotactic frame: (A) Top cross member. (B) Yoke. (C) Graphite support bar. An identical bar is present on the other side of the frame. A fiducial marker is present on each bar. (D) Sideplates with fiducial markers. The clear lucite sideplates have two grooves machined at right angles. Fine copper wires glued into the grooves serve as markers for angiograms and CT; these wires are imaged on lateral radiographs. For MRI, fine tubes filled with olive oil are substituted into the grooves. (E) Arch with fiducial markers. The arch supports two copper wire markers (or oil-tube markers for MRI) that are imaged on anteroposterior radiographs. (F) Positioning pins. The mask is reliably positioned with respect to the stereotactic frame by means of carefully placed holes that correspond to the three pins. (*From* Lyman JT, Phillips MH, Frankel KA, Fabrikant JI: Stereotactic frame for neuroradiology and charged particle Bragg peak radiosurgery of intracranial disorders. Int J Radiat Oncol Biol Phys 16:1617, 1989.) [CBB 877-5479A "with overlay"]

Fig. 9–5. Schematic diagram of charged-particle-beam delivery system at the University of California at Berkeley - Lawrence Berkeley Laboratory for stereotactic radiosurgery

of intracranial tumors and vascular disorders. The stereotactic patient-positioning system (ISAH) allows translation along three orthogonal axes (x,y,z) and rotation about the y and z axes, thereby providing precise patient immobilization and positioning for stereotactically directed charged-particle-beam therapy. The width of the high-dose Bragg ionization peak within the brain can be spread to the prescribed size by interposing a modulating filter of comparable maximum thickness (x cm) in the beam path, schematically shown here as a variable-thickness propeller. The range in tissue of the Bragg-peak region is determined by a range-modifying absorber. At the Bevatron accelerator, the range and modulation of the Bragg peak are controlled by use of a variable-position water-column absorber. An individually designed aperture specifically tailored to the size and configuration of the intracranial lesion shapes the beam in cross-section. Tissue-equivalent compensators further improve the precision placement of the high-dose Bragg-peak region by adjusting for irregular target contours, skull curvature and tissue inhomogeneities. Ion chambers monitor the dose delivered in each beam. Multiple entry angles and beam ports are chosen with appropriate modification of radiation parameters so that the high-dose regions of the individual beams intersect within the defined intracranial target (here, an arteriovenous malformation), with the lowest possible dose to sensitive adjacent normal brain tissues. (*From* Levy RP, Fabrikant JI, Frankel KA, Phillips MH, Lyman JT: Stereotactic heavy-charged-particle Bragg peak radiosurgery for the treatment of intracranial arteriovenous malformations in childhood and adolescence. Neurosurgery 24:842, 1989.) [XBL 8810-7674]

Fig. 9–6. Computer-reformatted overlay of digitized angiographic films for treatment-planning procedures, used to transfer the three-dimensional target volume for dose localization and to align the patient for the radiosurgical procedure. The overlay maps target contours, midplane bony landmarks, fiducial markers from the stereotactic frame and the isocenter of the patient positioner (denoted by the cross). **Upper**, lateral and anteroposterior views demonstrate the relative orientation of these elements when the stereotactic frame center is located at the isocenter of ISAH; note the perfect alignment of fiducial

markers on lateral view (**upper left**). **Lower**, corresponding views demonstrate the relative orientation when the patient has been moved so as to place the center of the lesion at the isocenter of the immobilization system ("treatment position"). The two concentric target contours reflect the angiographically derived target contour magnified to match the localization radiograph (outer contour) and the actual size of the AVM (inner contour), respectively. (*From* Phillips MH, Frankel KA, Lyman JT, Fabrikant JI, Levy RP: Heavy charged-particle stereotactic radiosurgery: Cerebral angiography and CT in the treatment of intracranial vascular malformations. Int J Radiat Oncol Biol Phys 17:423, 1989.) [XBL 888-2832]

Fig. 9–7. Stereotactic helium-ion Bragg-peak radiosurgery treatment plan for a 12-year-old girl with an arteriovenous malformation (AVM) of the brain stem (inner ring of white dots). Isodose contours have been calculated at 10, 50, 80 and 100% of the maximum dose in the axial (**left**) and coronal (**right**) planes. The 100% contour conforms precisely to the periphery of the lesion. There is a very rapid fall-off in dose outside the AVM target volume. Since four noncoplanar beams are used, very little normal brain tissue receives even as much as 10% of the dose to the AVM and most of the brain receives no radiation at all. There is virtually complete sparing and protection of midbrain and pontine structures. The helium-ion beam was collimated by an elliptical brass aperture measuring 8.5 x 11.5 mm; treatment was performed using four ports in 1 day, to a volume of 0.3 cm^3 (dose, 25 GyE). (*From* Levy RP, Fabrikant JI, Frankel KA, Phillips MH, Lyman JT: Stereotactic heavy-charged-particle Bragg peak radiosurgery for the treatment of intracranial arteriovenous malformations in childhood and adolescence. Neurosurgery 24:843, 1989.) [XBB 885-5361A]

Fig. 9–8. Stereotactic helium-ion Bragg-peak radiosurgery treatment plan for a large (54 cm^3) left temporal and deep central nuclei arteriovenous malformation in a 39-year-old man. **Left**, axial plane; **right**, sagittal plane. The helium-ion beam was collimated by

61 x 50 mm and 55 x 42 mm individually shaped brass and cerrobend apertures; 27 GyE was delivered in 3 days to the lesion (defined by the ring of white dots) using four noncoplanar beams. Isodose contours have been calculated for 10, 30, 50, 70, 90 and 99% of the maximum dose. The 90% isodose contour borders precisely on the periphery of the lesion. There is rapid dose fall-off to the 70% level, and the 10% isodose contour completely spares irradiation of the contralateral hemisphere. (*From* Fabrikant JI, Levy RP, Steinberg GK, Phillips, MH, Frankel KA, Lyman JT, Marks MP, Silverberg GD: Charged-particle radiosurgery for intracranial vascular malformations. Neurosurg Clin North Am 3:110, 1992.) [XBB 878-6973A]

Fig. 9–9. Stereotactic helium-ion Bragg-peak radiosurgery treatment plan for a 29-year-old woman with a symptomatic angiographically occult vascular malformation in the pons. **Left (upper and lower)**, diagnostic stereotactic MRI scans in the axial and sagittal planes are used to define the target volume (ring of white dots) for stereotactic radiosurgery. **Middle (upper and lower)**, the target contour data then are transferred to corresponding stereotactic CT images for treatment planning and calculation of isodose contours for display. **Right (upper and lower)**, the isodose-contour information then is transferred back to the original MRI scans to permit the explicit demonstration (and modification, where required) of isodose-contour distributions in all desired anatomic planes. Isodose contours displayed here in the axial and sagittal planes are calculated for 10, 50, 70 and 90% of the maximum central dose. (*From* Fabrikant JI, Levy RP, Steinberg GK, Phillips, MH, Frankel KA, Lyman JT, Marks MP, Silverberg GD: Charged-particle radiosurgery for intracranial vascular malformations. Neurosurg Clin North Am 3:112, 1992.) [XBB 898-7352]

Fig. 9–10. MRI scans of the pituitary region of a 49-year-old woman 14 years after transsphenoidal hypophysectomy for acromegaly. Recurrent acromegalic tumor is present with extension into the left cavernous sinus, lying directly on the left internal carotid artery.

Upper, coronal views demonstrate the tumor and its relationship to the optic nerves, chiasm and tracts, left carotid artery and adjacent cranial nerves. The tumor and cranial nerves are outlined for radiosurgical treatment planning. **Lower**, sagittal views demonstrate the precise distance between the upper edge of the tumor (outlined) and the optic chiasm. The MRI technique is part of the treatment-planning procedure for stereotactic charged-particle radiosurgery (cf Fig. 9–11). (*From* Levy RP, Fabrikant JI, Frankel KA, Phillips MH, Lyman JT: Charged-particle radiosurgery of the brain. Neurosurg Clin North Am 1:972, 1990.) [XBB 898-6688A]

Fig. 9–11. Stereotactic helium-ion Bragg-peak radiosurgery treatment plan for the recurrent acromegalic tumor in the patient illustrated in Fig. 9–10. The radiosurgical target is defined by the inner ring of white dots. The helium-ion Bragg peak was modulated 0.5 cm, and it was collimated by a 15 x 13 mm elliptical brass aperture. A dose of 30 GyE was delivered to a volume of 0.8 cm^3 through eight ports in 1 day. Isodose contours are calculated for 10, 20, 30, 50, 70, 90 and 95% of the maximum central dose in the axial (**upper**) and coronal (**lower**) planes. The 5% isodose contour is also calculated in the coronal plane and demonstrates the rapid fall-off of dose within a few millimeters of the irradiated target volume. The treatment plan was designed to minimize dose to the cavernous sinus while placing a higher dose in the tumor mass lying within the sella. The optic chiasm, nerves and tracts received less than 10% of the central dose, i.e., less than 3 GyE, and the parasellar cranial nerves only a fraction of this dose. (*From* Levy RP, Fabrikant JI, Frankel KA, Phillips MH, Lyman JT: Charged-particle radiosurgery of the brain. Neurosurg Clin North Am 1:973, 1990.) [XBB 898-6680]

Fig. 9–12. Stereotactic positioning table and head holder for plateau-beam helium-ion pituitary-irradiation system developed at the University of California at Berkeley - Lawrence Berkeley Laboratory 184-inch synchrocyclotron. The mask is a rigid transparent polystyrene unit which is tailored for each patient. During irradiation, the patient is posi-

tioned sequentially at 12 discrete angles, covering a 66° arc around the vertical (y) axis; at each position, the patient's head is turned in pendulum motion through a 70° arc around the horizontal (x) axis. (*From* Levy RP, Fabrikant JI, Frankel KA, Phillips MH, Lyman JT: Charged-particle radiosurgery of the brain. Neurosurg Clin North Am 1:971, 1990.) [JHL 2897-C "with overlay"]

Fig. 9–13. Three-dimensional isodose contours for one octant of the radiation field used to treat pituitary adenomas at the University of California at Berkeley - Lawrence Berkeley Laboratory 184-inch synchrocyclotron (cf Fig. 9–12). Stereotactic irradiation is performed with the plateau-ionization portion of the 230 MeV/u helium-ion beam. The dose fall-off from 90% to 10% occurs in less than 4 mm in the frontal plane. The technique produces very favorable dose distributions for the treatment of small intracranial lesions. (*From* Tobias CA: Pituitary radiation: Radiation physics and biology. *In* Linfoot JA (ed): Recent Advances in the Diagnosis and Treatment of Pituitary Tumors. New York, Raven Press, 1979, pg 234.) [MU-14976]

Fig. 9–14. Treatment plan for a large irregular thalamic arteriovenous malformation (AVM). Milled wax compensators for each beam port, designed with computer assistance on a CT-slice-by-slice basis, were used to align the distal edge of the Bragg peak to the distal surface of the AVM (defined by the ring of white dots; volume, 17 cm^3). Isodose contours, calculated for 10, 30, 50, 70, 90 and 99% of the maximum central dose, are illustrated for a single CT slice. The 165 MeV/u helium-ion beam was collimated by individually shaped cerrobend apertures. A dose of 20 GyE was delivered to the lesion using four coplanar beam ports in 2 days. [XBB 923-1690]

Fig. 9–15. **Left**, isodose contours (10, 50, 70, 90 and 99%) are illustrated for the posterior beam-port component of the composite (multi-port) treatment plan shown in Fig. 9–14. The target (defined by the ring of white dots) was irradiated with a *fixed* spread-out Bragg-peak (SOBP) value of 3.5 cm for this beam port. In this treatment configuration, significant

portions of the right thalamus and adjacent brain stem are irradiated to the full treatment dose (5 GyE) from this beam port. (In practice, the dose to these sensitive structures is reduced by irradiating the target from multiple angles.) **Right**, the corresponding single-port treatment plan for a *scanned* beam with a *variable* SOBP is illustrated for comparison. The treatment-planning program for beam scanning adjusts the value of the SOBP so that only the target volume receives the maximum dose (see text); with this method, the dose to sensitive adjacent structures is less than would occur using a beam with a fixed SOBP. [XBB 928-6621A]

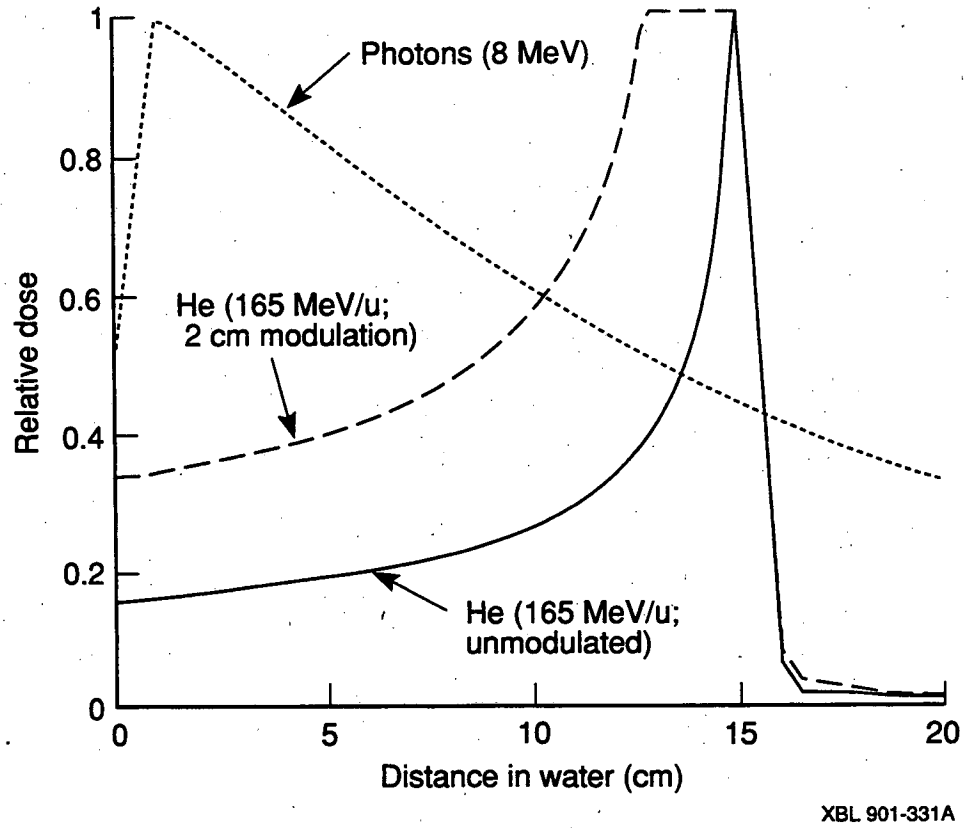
Photons (8 MeV)
He (165 MeV/u;
2 cm modulation)
He (165 MeV/u;
unmodulated)
Relative dose
1
0.8
0.6
0.4
0.2
0
0
5
10
15
20
Distance in water (cm)
XBL 901-331A

Fig. 9-1

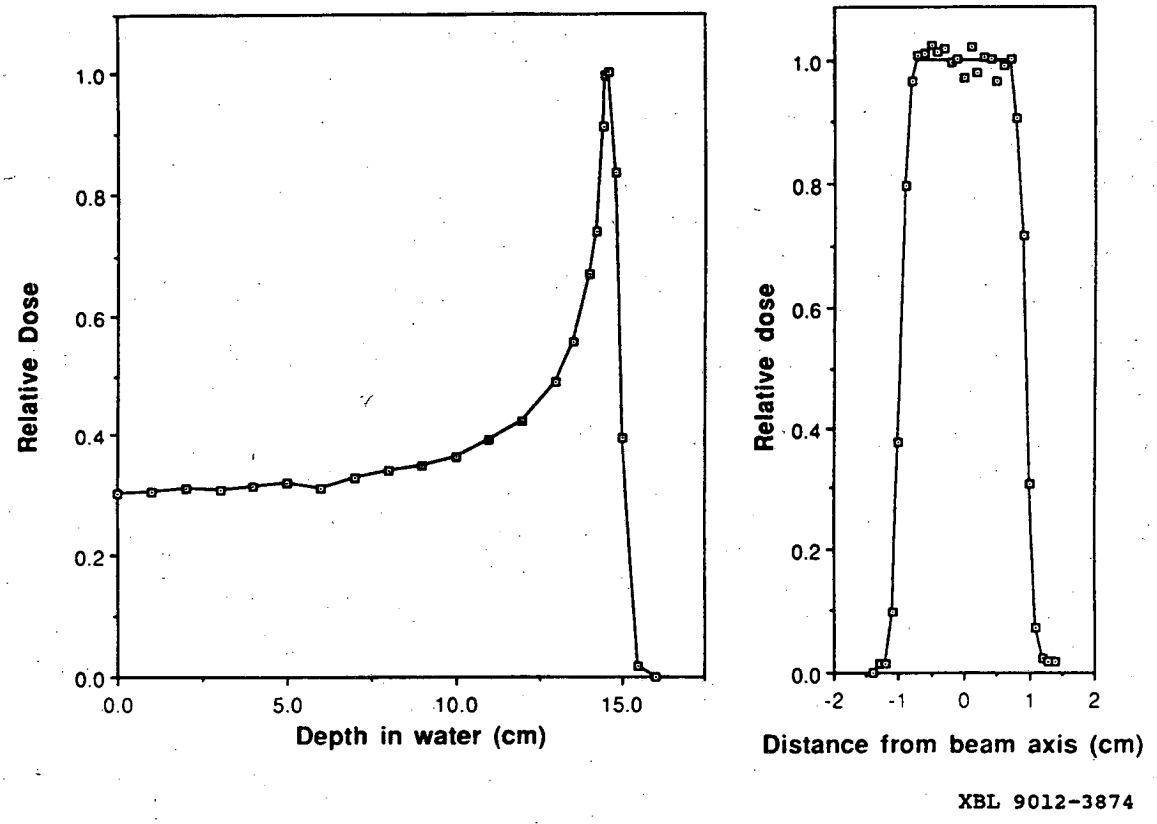
Relative Dose
1.0
0.8
0.6
0.4
0.2
0.0
0.0
5.0
10.0
15.0
Depth in water (cm)
Relative dose
1.0
0.8
0.6
0.4
0.2
0.0
-2
-1
0
1
2
Distance from beam axis (cm)
XBL 9012-3874

Fig. 9-2

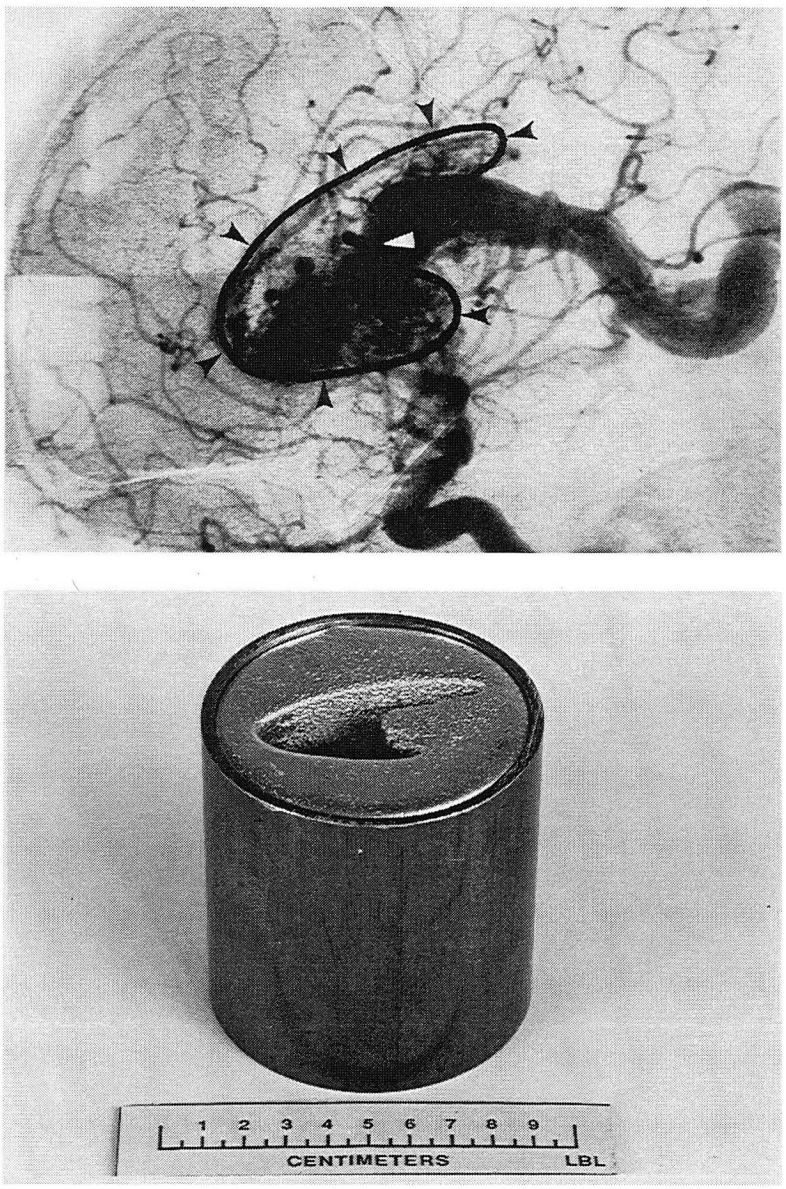

XBB 901-795A

Fig. 9-3

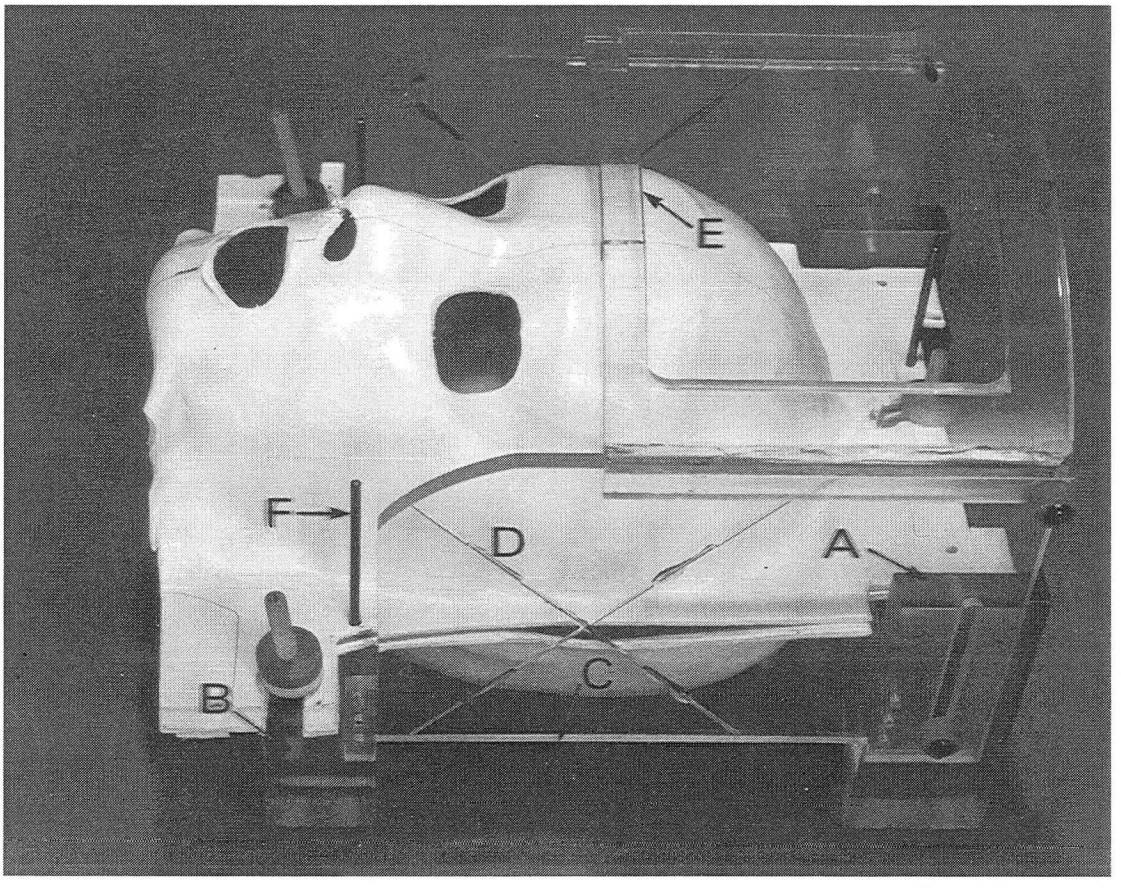

CBB 877-5479A

Fig. 9-4

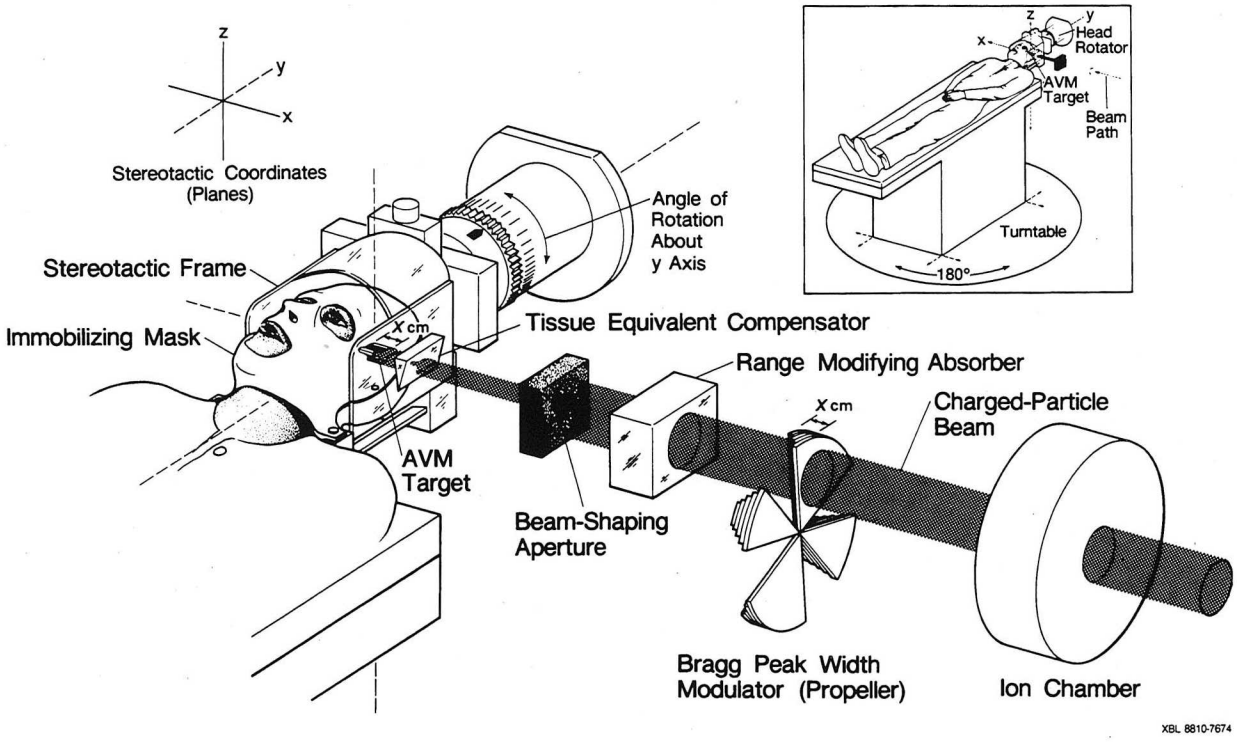
Charged Particle Beam Delivery System
z
y
x
Stereotactic Coordinates
(Planes)
Stereotactic Frame
Immobilizing Mask
X cm
AVM
Target
Angle of
Rotation
About
y Axis
Tissue Equivalent Compensator
Range Modifying Absorber
Beam-Shaping
Aperture
X cm
Charged-Particle
Beam
Bragg Peak Width
Modulator (Propeller)
Ion Chamber
z
y
x
Head
Rotator
AVM
Target
Beam
Path
Turntable
180°
XBL 8810-7674

Fig. 9-5

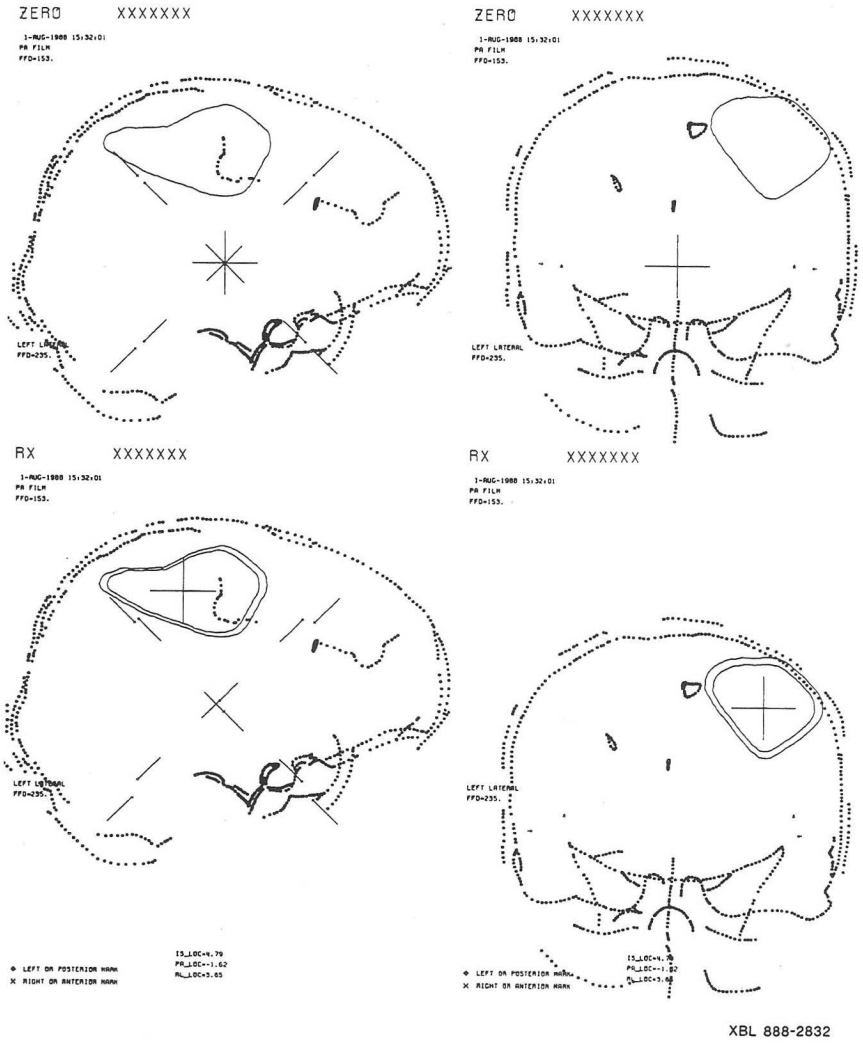
ZERO XXXXXXX
1-AUG-1988 15:32:01
PA FILM
FFD=153.
LEFT LATERAL
FFD=235.
RX XXXXXXX
1-AUG-1988 15:32:01
PA FILM
FFD=153.
LEFT LATERAL
FFD=235.
IS_LOC=4.79
PA_LOC=-1.62
RL_LOC=3.65
◆ LEFT OR POSTERIOR MARK
✕ RIGHT OR ANTERIOR MARK
XBL 888-2832

Fig. 9-6

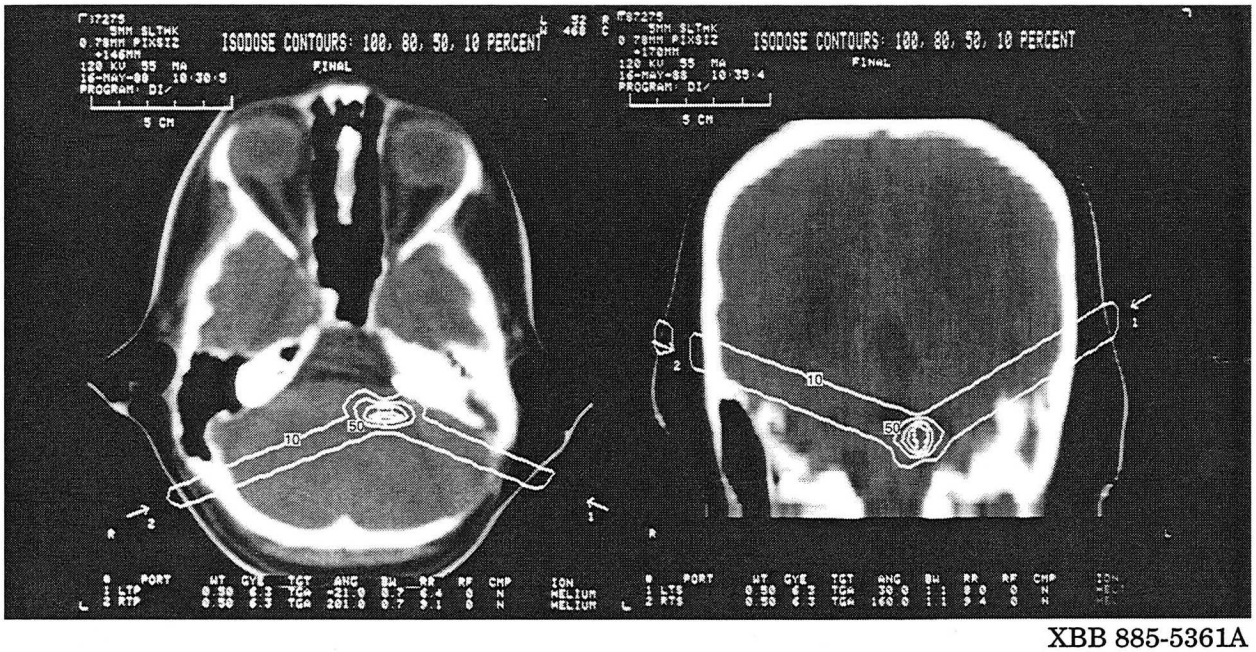

XBB 885-5361A

Fig. 9-7

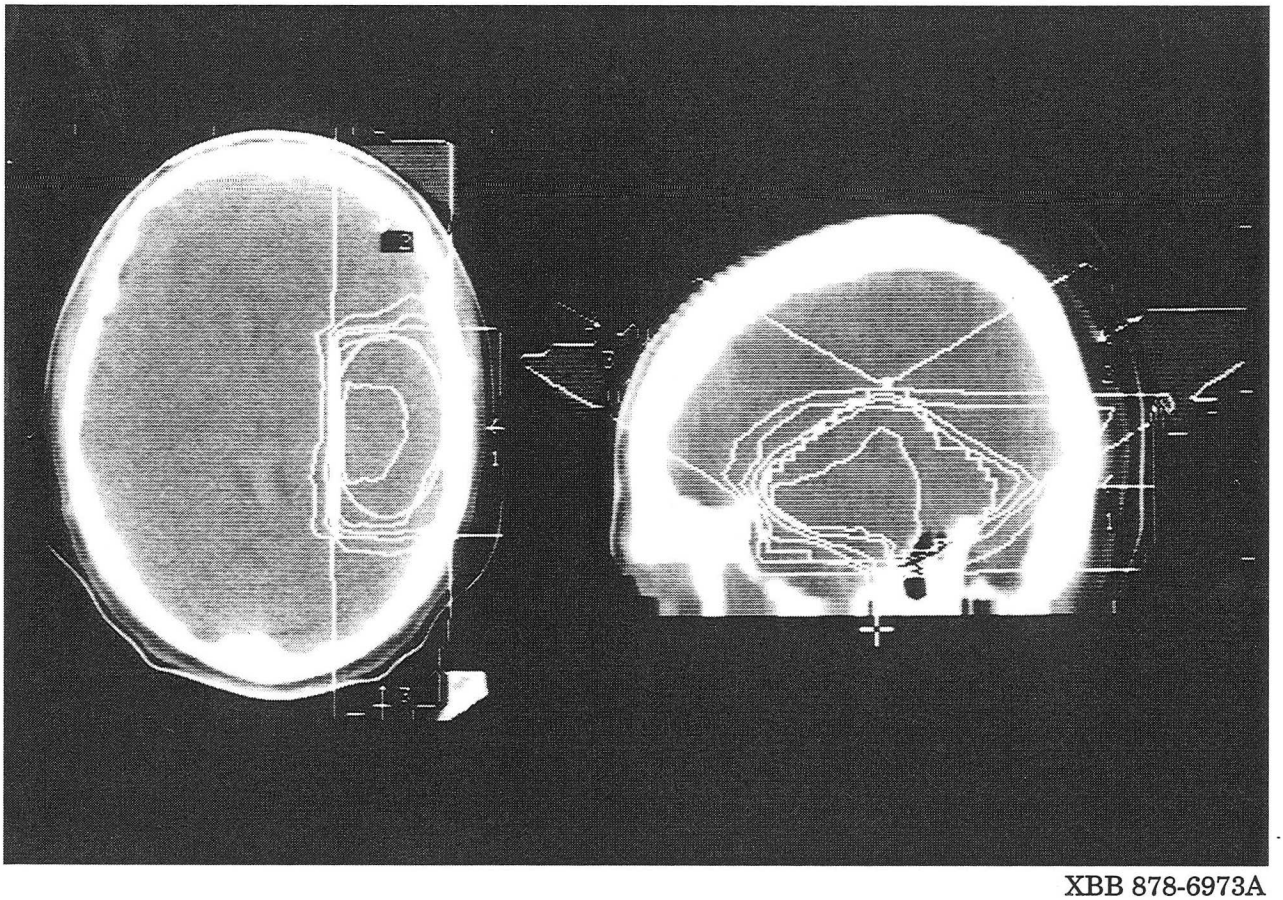

XBB 878-6973A

Fig. 9-8

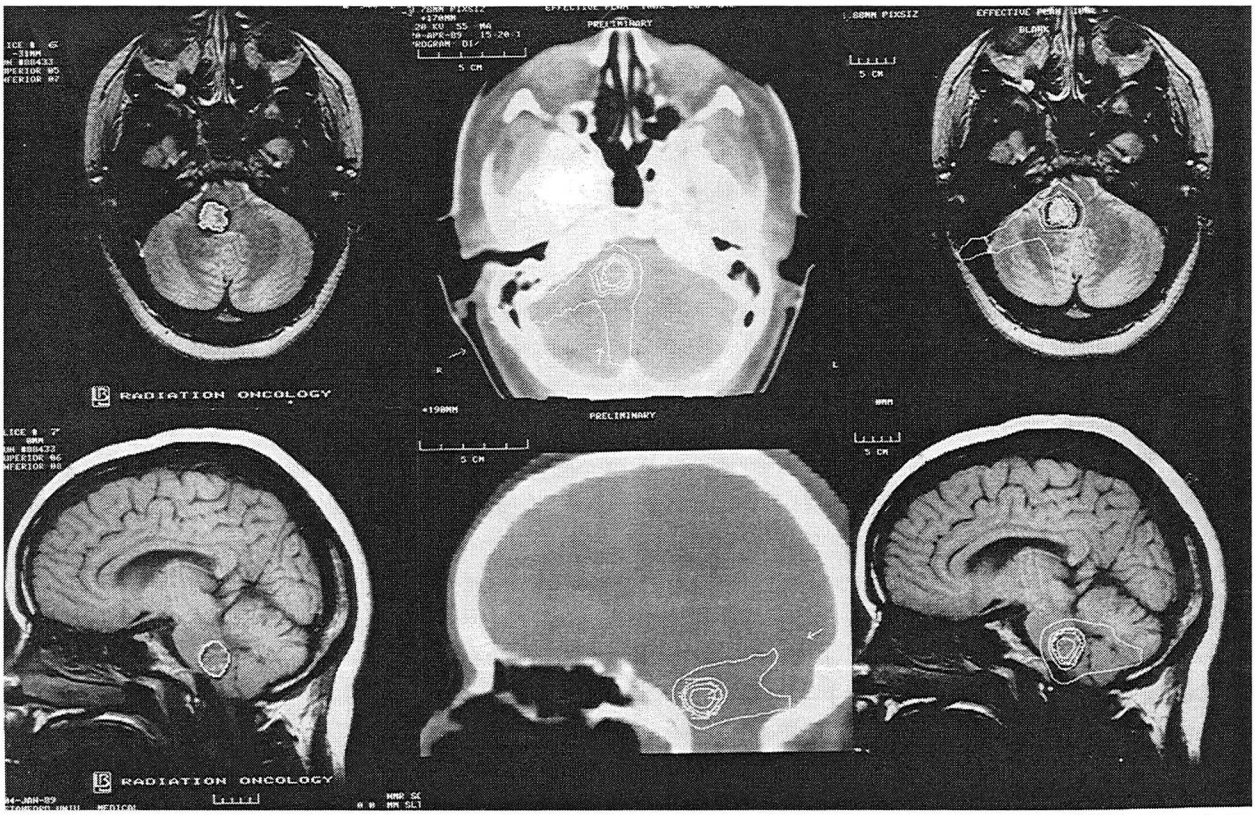

XBB 899-7352

Fig. 9-9

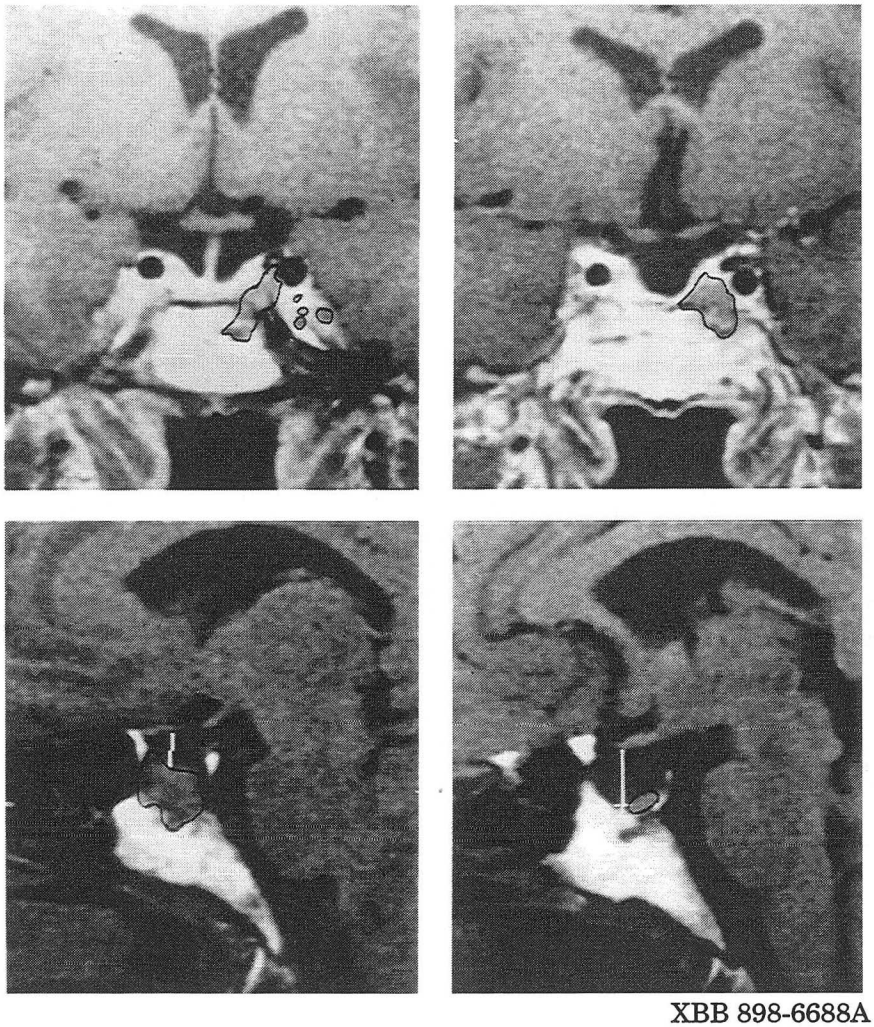

XBB 898-6688A

Fig. 9-10

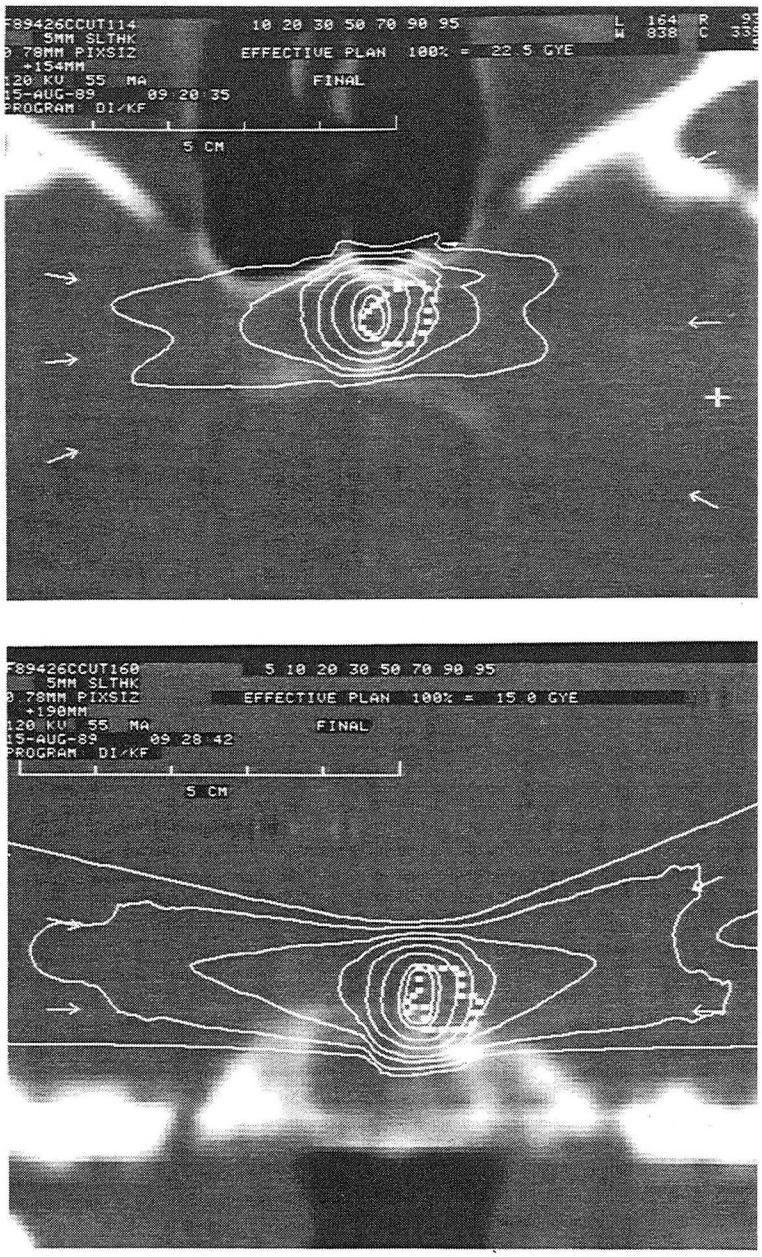

XBB 898-6680

Fig. 9-11

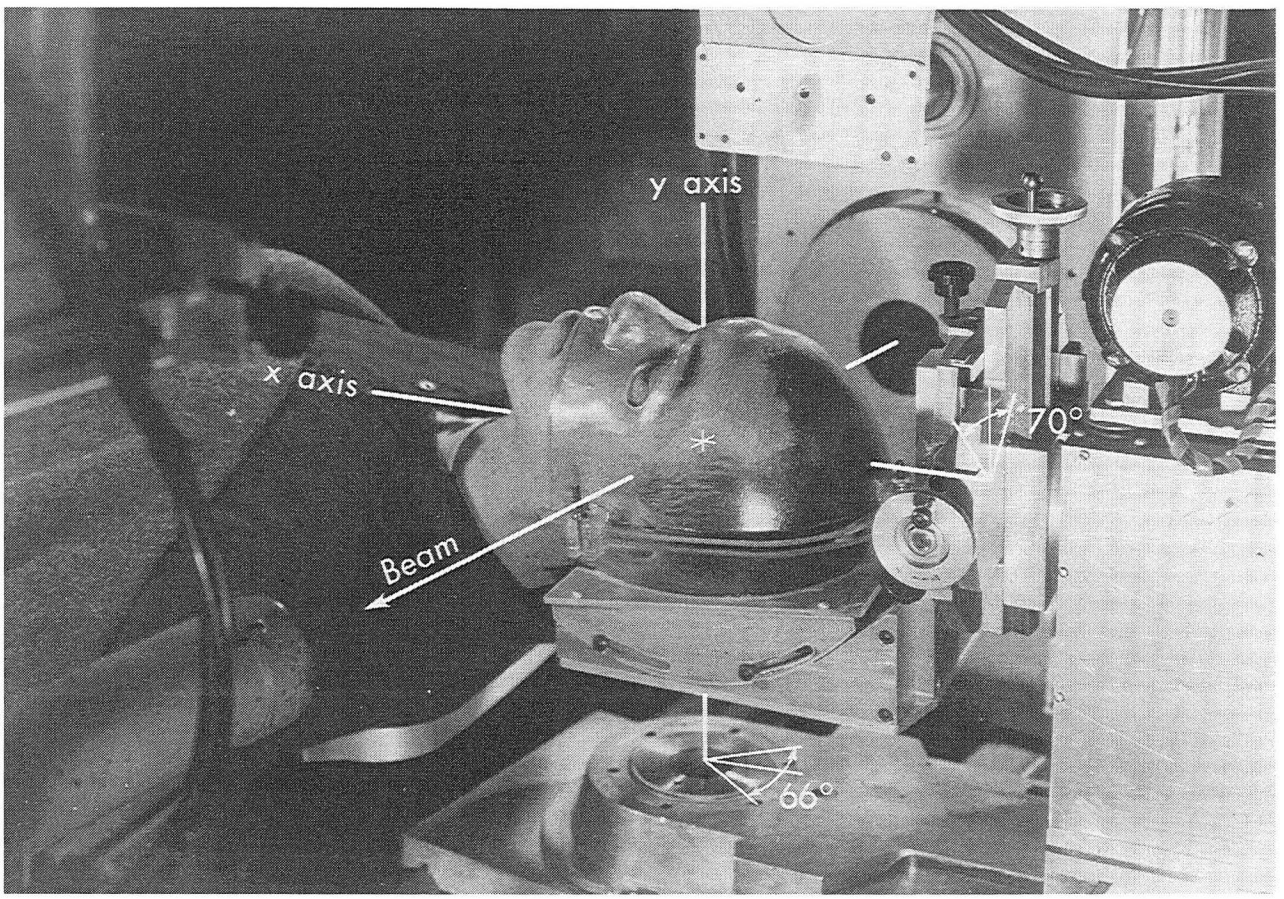

JHL 2897C

Fig. 9-12

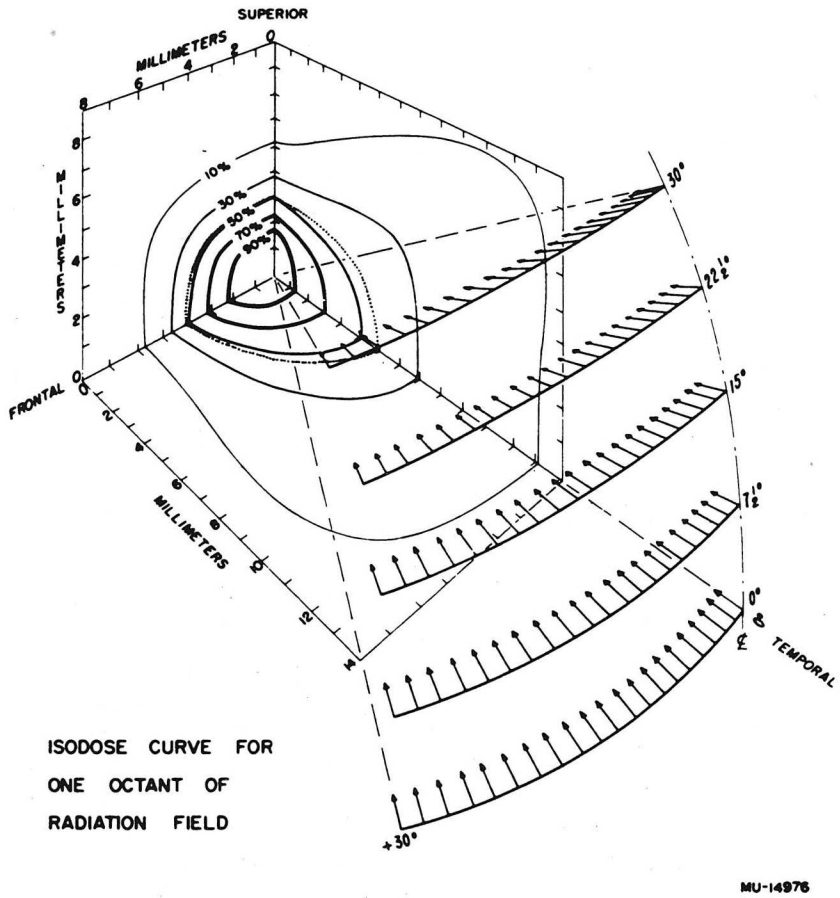
SUPERIOR
MILLIMETERS
0
2
4
6
8
10%
30%
50%
70%
90%
FRONTAL
MILLIMETERS
0
2
4
6
8
10
12
14
30°
22½°
15°
7½°
0°
TEMPORAL
+30°
ISODOSE CURVE FOR
ONE OCTANT OF
RADIATION FIELD
MU-14976

Fig. 9-13

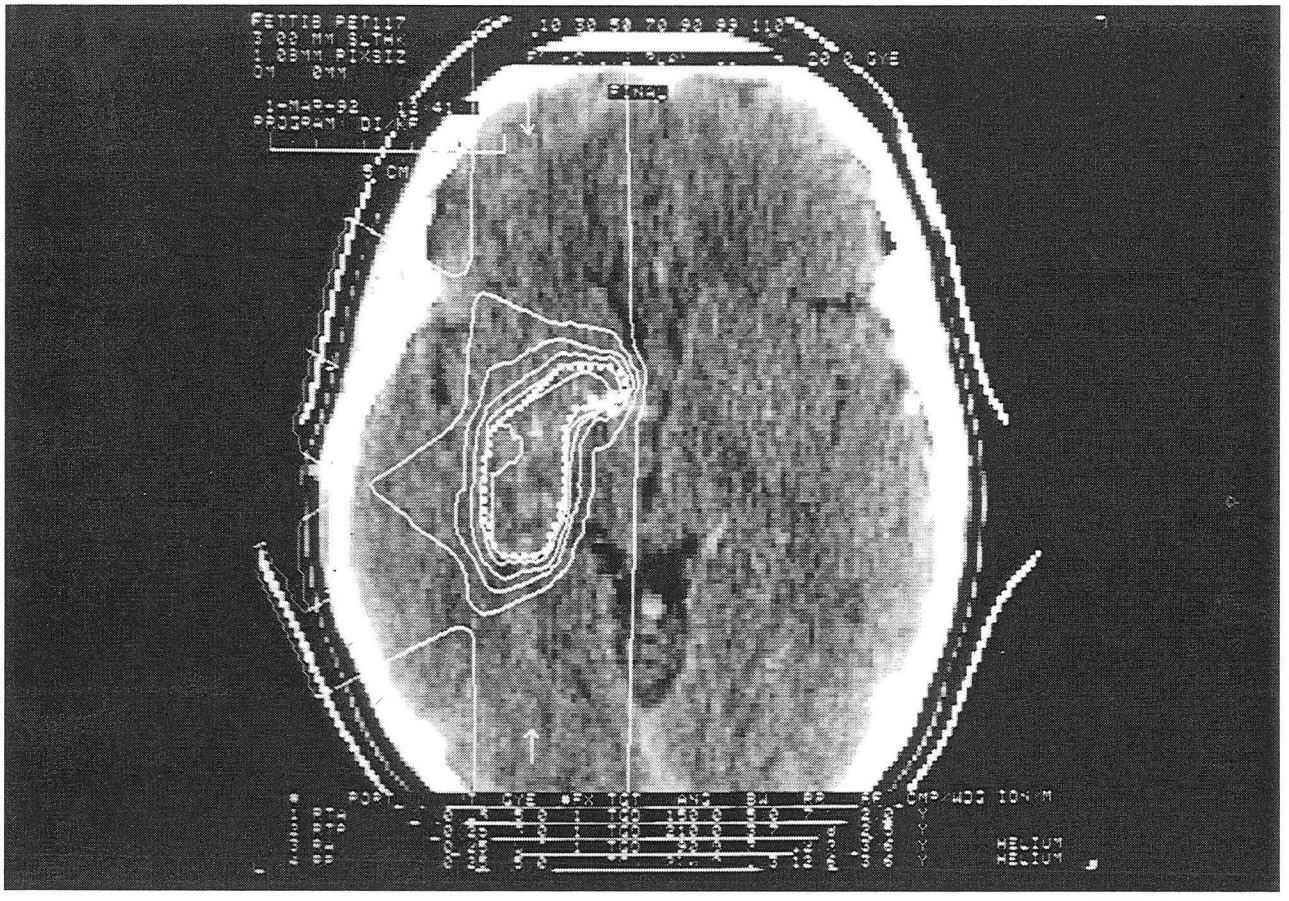

XBB 923-1690

Fig. 9-14

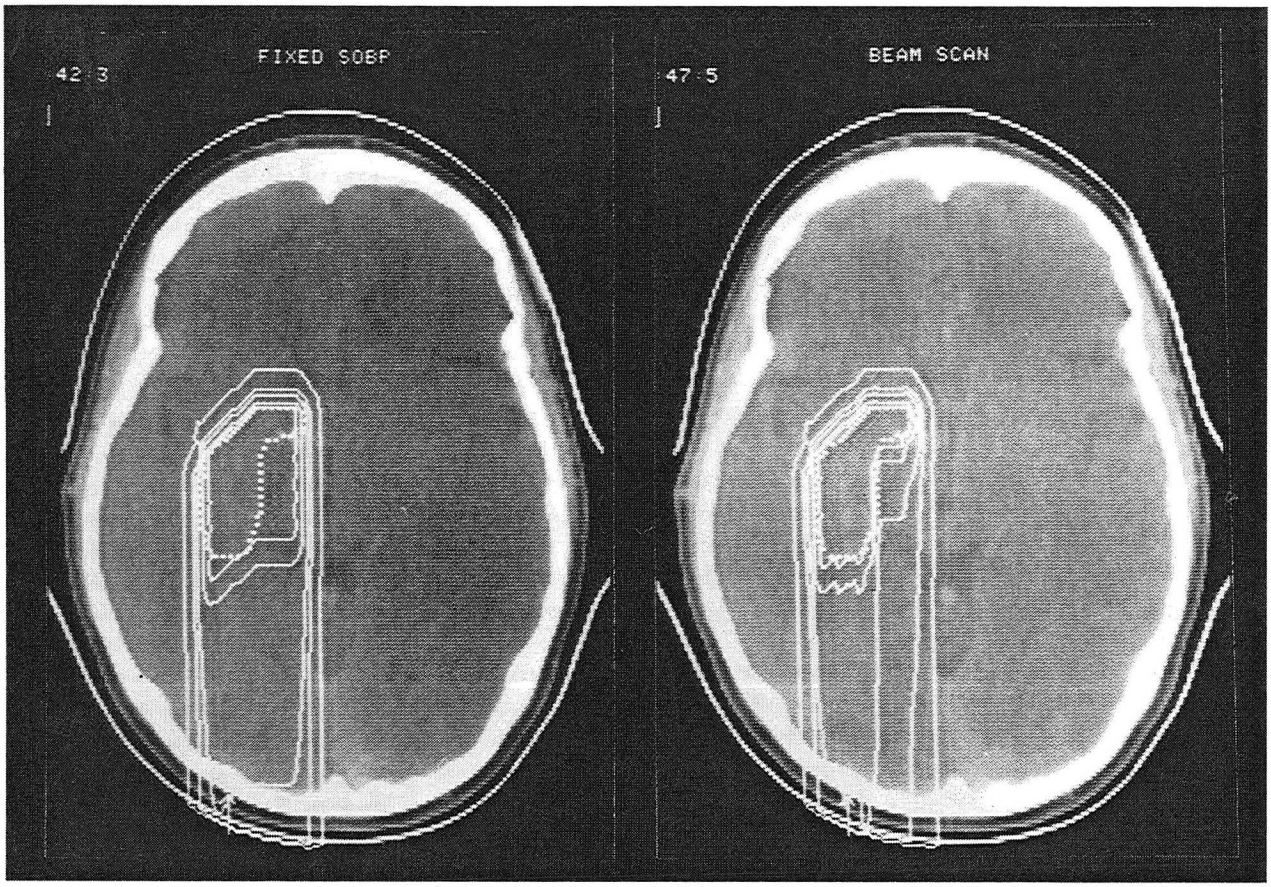

XBB 928-6621A

Fig. 9-15

LAWRENCE BERKELEY LABORATORY
UNIVERSITY OF CALIFORNIA
TECHNICAL INFORMATION DEPARTMENT
BERKELEY, CALIFORNIA 94720